# Oxygen-dependent asparagine hydroxylation of the ubiquitin-associated (UBA) domain in Cezanne regulates ubiquitin binding

Received for publication, July 23, 2019, and in revised form, December 27, 2019 Published, Papers in Press, January 14, 2020, DOI 10.1074/jbc.RA119.010315

**Julia Mader[‡], Jessica Huber[§], Florian Bonn[‡], Volker Dötsch[§], Vladimir V. Rogov[§], and Anja Bremm[‡1]**

*From the [‡]Institute of Biochemistry II, Faculty of Medicine, Goethe University Frankfurt, Theodor-Stern-Kai 7, 60590 Frankfurt am Main, Germany and the [§]Institute of Biophysical Chemistry and Center for Biomolecular Magnetic Resonance, Goethe University Frankfurt, Max-von-Laue Strasse 9, 60438 Frankfurt am Main, Germany*

Edited by George N. DeMartino

**Deubiquitinases (DUBs) are vital for the regulation of ubiquitin signals, and both catalytic activity of and target recruitment by DUBs need to be tightly controlled. Here, we identify asparagine hydroxylation as a novel posttranslational modification involved in the regulation of Cezanne (also known as OTU domain–containing protein 7B (OTUD7B)), a DUB that controls key cellular functions and signaling pathways. We demonstrate that Cezanne is a substrate for factor inhibiting HIF1 (FIH1)- and oxygen-dependent asparagine hydroxylation. We found that FIH1 modifies $Asn^{35}$ within the uncharacterized N-terminal ubiquitin-associated (UBA)-like domain of Cezanne ($UBA^{Cez}$), which lacks conserved UBA domain properties. We show that $UBA^{Cez}$ binds $Lys^{11}$-, $Lys^{48}$-, $Lys^{63}$-, and $Met^{1}$-linked ubiquitin chains *in vitro*, establishing $UBA^{Cez}$ as a functional ubiquitin-binding domain. Our findings also reveal that the interaction of $UBA^{Cez}$ with ubiquitin is mediated via a noncanonical surface and that hydroxylation of $Asn^{35}$ inhibits ubiquitin binding. Recently, it has been suggested that Cezanne recruitment to specific target proteins depends on $UBA^{Cez}$. Our results indicate that $UBA^{Cez}$ can indeed fulfill this role as regulatory domain by binding various ubiquitin chain types. They also uncover that this interaction with ubiquitin, and thus with modified substrates, can be modulated by oxygen-dependent asparagine hydroxylation, suggesting that Cezanne is regulated by oxygen levels.**

Deubiquitinases (DUBs)[2] are essential players in the ubiquitin system. They reverse and shape ubiquitin signals and hence control the complex ubiquitin code and its cellular consequences (1). Deregulation of DUBs has been linked to a variety of diseases like cancer, neurodegeneration, and inflammatory diseases. To safeguard proper DUB function, multiple layers of regulatory mechanisms evolved in the cell, which ensure the correct abundance and localization of DUBs or directly regulate their catalytic activity (2). Among others, posttranslational modifications (PTMs) and accessory domains within DUBs are employed to control DUB function.

Cezanne (OTUD7B) is a member of the ovarian tumor protease (OTU) family, and its catalytic OTU domain targets $Lys^{11}$-linked ubiquitin chains with high selectivity (3, 4). Structural studies of the OTU domain alone and in complex with $Lys^{11}$-linked diubiquitin suggest that Cezanne is autoinhibited in the absence of ubiquitin. The OTU domain contacts the distal molecule of all chain types via an exposed S1 site. However, an S1′ site is not present until $Lys^{11}$-linked diubiquitin is bound across the active site (4). These conformational rearrangements upon diubiquitin binding explain the selectivity of the OTU domain for $Lys^{11}$-linked ubiquitin chains.

Although the structural and biochemical properties of Cezanne's catalytic OTU domain have been extensively characterized *in vitro*, the functional role of the additional two ubiquitin-binding domains (UBDs) and of the almost 50% of a Cezanne molecule that is predicted to be unstructured remain elusive. One study linked the C-terminal A20-type zinc finger (ZnF) to the inhibition of ligand-dependent EGF receptor degradation by Cezanne (5), and a recent publication suggested a role for the N-terminal ubiquitin-associated (UBA)-like domain in recruitment of Cezanne to activated TNF receptor complex (6). During the last decade, Cezanne has been associated with multiple cellular processes, including the regulation of NF-κB (7, 8),

This work was supported by German Research Foundation Grants BR 4268/2-1 (to A. B.) and CRC/SFB 1177 on selective autophagy (to F. B.). The authors declare that they have no conflicts of interest with the contents of this article.
This article was selected as one of our Editors' Picks.
This article contains Figs. S1–S7.
*The mass spectrometry proteomics data have been deposited to the ProteomeXchange Consortium via the PRIDE partner repository with the data set identifier PXD015216.*
*Spectra of hydroxylated peptides have been uploaded to MS-Viewer with search keys thxk27wtoe for the SILAC-labeled sample and li99oswlz9 for the bacterial expressed protein.*
*NMR data have been deposited to the Biological Magnetic Resonance Data Bank (BMRB), entry 27984.*
[1] To whom correspondence should be addressed: Institute of Biochemistry II, Faculty of Medicine, Goethe University Frankfurt, Theodor-Stern-Kai 7, 60590 Frankfurt am Main, Germany. Tel.: 49-69-6301-5450; Fax: 49-69-6301-5287; E-mail: bremm@em.uni-frankfurt.de.


[2] The abbreviations used are: DUB, deubiquitinase; IPTG, isopropyl β-D-thiogalactopyranoside; PTM, posttranslational modification; OTU, ovarian tumor protease; UBD, ubiquitin-binding domain; ZnF, zinc finger; EGF, epidermal growth factor; UBA, ubiquitin-associated; KO, knockout; GST, glutathione *S*-transferase; CSP, chemical shift perturbation(s); DMEM, Dulbecco's modified Eagle's medium; PEI, polyethyleneimine; PMSF, phenylmethylsulfonyl fluoride; IP, immunoprecipitation; PD, pulldown; HSQC, heteronuclear single quantum coherence spectroscopy; SILAC, stable isotope labeling by amino acids in cell culture; SDC, sodium desoxychelate; HRP, horseradish peroxidase; PDB, Protein Data Bank.

hypoxia signaling (9), mTORC2 signaling (10), and human cell cycle progression (11). Interestingly, Cezanne-dependent cleavage of ubiquitin chain types conjugated to respective substrates has not always been in accordance with former *in vitro* studies. Some reports have suggested that in addition to $Lys^{11}$-linked polyubiquitin, full-length Cezanne can also process $Lys^{48}$- and $Lys^{63}$-linked ubiquitin chains *in vivo* (8, 10). However, it is not yet understood whether Cezanne's ability to cleave linkage types other than $Lys^{11}$ in a cellular context depends on cofactors present in the cell, on an acute increase in local concentrations of Cezanne that would allow cleavage of different chain types ("proximity effect"), or on distinct regions within the full-length enzyme itself. Therefore, studying the accessory domains of Cezanne like the UBA domain ($UBA^{Cez}$) will add to our understanding of how modified substrates are discriminated by Cezanne.

UBA domains are short sequence motifs of ~45 amino acids that adopt a compact three-helix bundle. Like other UBDs, UBA domains recognize ubiquitinated substrates via interaction with ubiquitin and serve to decode ubiquitin signals into a cellular response (12). Originally identified in shuttle factors, UBA domains have also been found in various other proteins, including autophagy receptors, E3 ubiquitin ligases, and DUBs. For most UBA domains, an unusually large hydrophobic surface patch has been described (13). The so-called MGF motif is highly conserved and part of the connecting loop between helix $\alpha$1 and $\alpha$2. The MGF motif is not required to maintain the local structure of the UBA domain but contributes to the hydrophobic surface patch for interaction with ubiquitin. In addition, a dileucine motif in helix $\alpha$3 is present in most UBA domains and involved in ubiquitin binding (13). With very few exceptions (*e.g.* the UBA domain of the E3 ubiquitin ligase Cbl-b (14, 15) or of the yeast protein Swa2p (16)), UBA domains engage the hydrophobic $Ile^{44}$ patch of ubiquitin via the same surface comprising MGF and LL motifs. Interestingly, the UBA domain of the autophagy receptor p62 needs to be phosphorylated to bind $Lys^{63}$-linked ubiquitin chains with sufficient affinity and to enable p62 to act as an autophagy receptor for ubiquitinated protein aggregates (17). This observation shows that the interaction between ubiquitin and UBA domains can be regulated by PTMs.

Our work presented here demonstrates that $UBA^{Cez}$ is posttranslationally modified by the asparaginyl $\beta$-hydroxylase factor inhibiting HIF1 (FIH1) and thereby associates a novel PTM with a UBD. Interestingly, in an MS-based interactome study, FIH1 was previously identified as a binding partner of Cezanne (18). FIH1 belongs to the family of 2-oxoglutarate and Fe(II)-dependent dioxygenases (19), and FIH1 is a key regulator of the cellular oxygen-sensing machinery that controls the transcriptional activity of hypoxia-inducible factor 1-$\alpha$ (HIF1$\alpha$). In the presence of oxygen, FIH1 hydroxylates a conserved asparagine residue in the C-terminal transactivation domain of HIF1$\alpha$, which blocks its interaction with the co-activator p300 (20, 21) and renders HIF1$\alpha$ inactive. In addition to HIF1$\alpha$, other targets of FIH1 have been described, most of them containing a common interaction motif known as the ankyrin repeat domain (22). For example, hydroxylation of apoptosis-stimulating p53-binding protein 2 (ASPP2), a regulator of apoptosis and cell polarity, impairs its association with partitioning-defective 3 homolog (PAR-3), which in turn results in relocation of ASPP2 from cell-cell contacts to the cytosol (23). Furthermore, FIH1-mediated hydroxylation inhibits the ion channel transient receptor potential vanilloid 3 (TRPV3) (24) and negatively regulates the interactome of the OTU family DUB OTUB1 (25). More recently, it has been shown that invading pathogens like *Legionella pneumophilia* exploit host FIH1-dependent asparagine hydroxylation by recruiting FIH1 to the pathogen-containing vacuole and that hydroxylation of translocated effector proteins are indispensable for their function (26). These examples illustrate the diversity of asparagine hydroxylation signals and how the addition of one oxygen atom can modulate protein-protein interactions.

Here, we identified a putative consensus site for FIH1-dependent hydroxylation in Cezanne. We confirmed the interaction between Cezanne and FIH1 by immunoprecipitation assays and revealed that Cezanne is posttranslationally hydroxylated at $Asn^{35}$ in an FIH1- and oxygen-dependent manner, establishing Cezanne as a novel substrate for FIH1. The modified asparagine residue is part of Cezanne's UBA domain ($UBA^{Cez}$), which belongs to the conserved protein domain family "UBA_like_SF" (cd14347) (27). However, the functionality of $UBA^{Cez}$ has never been proven. Our work showed that $UBA^{Cez}$ binds polyubiquitin of different linkage types (*e.g.* $Lys^{11}$, $Lys^{48}$, $Lys^{63}$, and linear/$Met^1$), although it lacks critical UBA domain features like the conserved MGF motif. NMR titration experiments revealed that $UBA^{Cez}$ binds monoubiquitin and linear diubiquitin via a noncanonical surface comprising helix $\alpha$2 and $\alpha$3, with $K_D$ values comparable with other described ubiquitin-UBD interactions. Importantly, hydroxylation of $Asn^{35}$ greatly reduced the interaction of $UBA^{Cez}$ with ubiquitin.

## Results

### *Cezanne harbors a FIH1 consensus site*

FIH1 selectively hydroxylates asparagine residues within the L*X*5(D/E)ΦNΦ motif (where Φ represents aliphatic amino acids) in multiple eukaryotic proteins. The addition of the strong electronegative oxygen atom to the $\beta$-carbon of asparagine residues increases the polarity of a protein and can act as a hydrogen bond donor and acceptor. Therefore, hydroxylation is an efficient intracellular tool to regulate protein-protein interactions (28). A global proteomic analysis of deubiquitinating enzymes and their associated protein complexes showed that FIH1 interacts with Cezanne (18). Furthermore, we identified a putative consensus site for FIH1-dependent hydroxylation in Cezanne (Fig. 1*A*). We have previously demonstrated that Cezanne is crucial for the HIF-dependent cellular adaptation to hypoxia and thus it interacts with the prime substrate of FIH1 (9, 29). Based on these findings, we hypothesized that Cezanne is a novel substrate for FIH1.

First, we confirmed and characterized the interaction between Cezanne and FIH1. Co-immunoprecipitation experiments demonstrated that FIH1 interacts with Cezanne in HEK293 cells (Fig. 1*B*). Interestingly, the catalytic inactive mutant FIH1 (H199A) and the dimerization-deficient mutant FIH1 (L340R) did not bind Cezanne (Fig. 1*C*). In the context of HIF1$\alpha$ regulation, it has been shown that disruption of FIH1

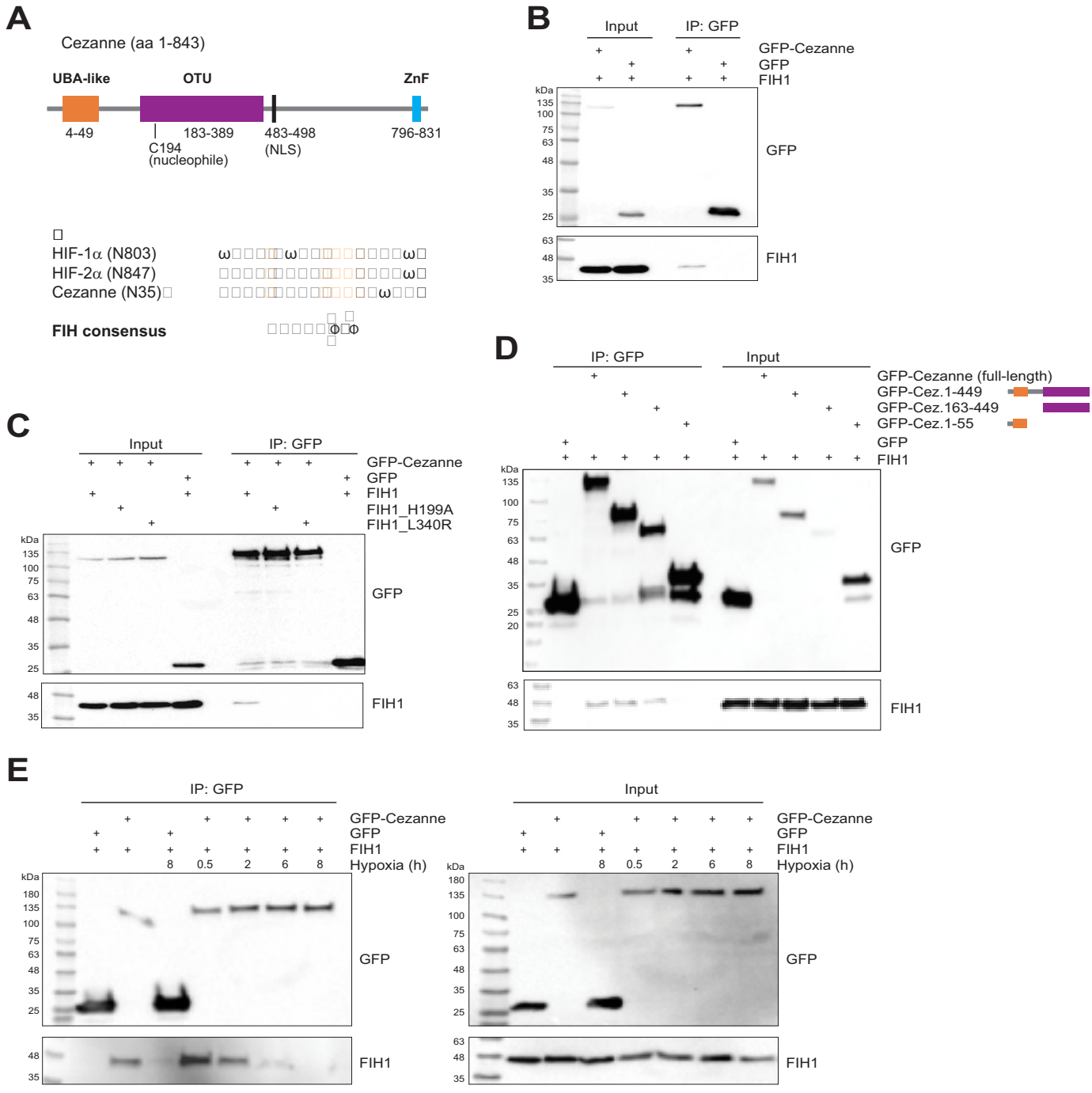


**Figure 1. Cezanne contains a putative consensus site for FIH1-dependent hydroxylation.** *A*, overview of the domain architecture of Cezanne and sequence alignment showing an FIH1 consensus sequence in Cezanne (where Φ indicates aliphatic amino acids and * represents the modified asparagine residue). *B*, co-IP of GFP-Cezanne and FIH1 from HEK293 cells. *C*, co-IP of GFP-Cezanne and catalytic inactive FIH1 (H199A) and dimerization-deficient FIH1 (L340R) mutants. *D*, co-IP of GFP-Cezanne truncated versions and FIH1 to narrow down the region in Cezanne that interacts with FIH1. *E*, co-IP of GFP-Cezanne and FIH1, assessing the effect of hypoxia on the interaction of the two proteins.

dimerization abolishes HIF1α binding and hydroxylation by FIH1 (30), further strengthening our hypothesis that Cezanne interacts with FIH1 as its substrate. Using truncated Cezanne variants, we mapped the minimal FIH1-binding region of Cezanne to the catalytic OTU domain (Fig. 1*D*). Another remarkable observation was that the interaction between Cezanne and FIH1 was lost when cells were exposed to hypoxia (1% oxygen) for 6–8 h (Fig. 1*E*), a condition in which FIH1 activity is decreased. Our results suggest that Cezanne is in complex with FIH1 and that this association depends on FIH1 hydroxylase activity.

### *The UBA domain of Cezanne is hydroxylated by FIH1*

Using SILAC-based MS, we tested whether Cezanne is indeed hydroxylated by FIH1. We generated CRISPR/Cas9-

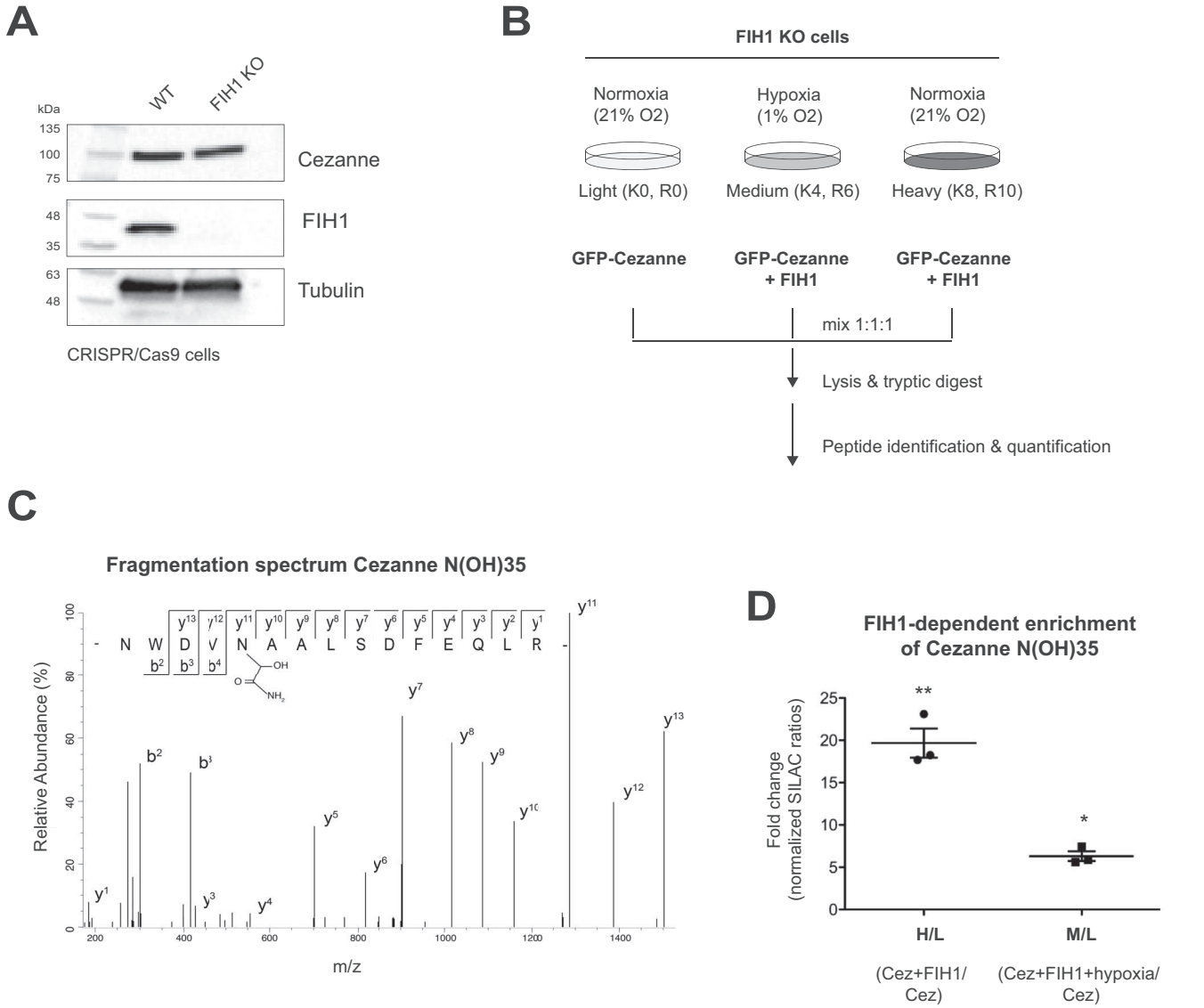


**Figure 2. Cezanne is hydroxylated within its UBA-like domain.** *A*, FIH1 was efficiently depleted by CRISPR/Cas9-mediated knockout in HEK293 cells. *B*, *cartoon* depicting design of SILAC-based MS experiment for the detection of asparagine hydroxylation in Cezanne. *C*, annotated MS2 spectrum showing hydroxylated Asn[35] of Cezanne in HEK293 cells. *D*, FIH1- and oxygen-dependent enrichment of Asn[35] hydroxylation. Data are represented as mean of SILAC ratios plus S.E. (*error bars*). *, $p < 0.1$; **, $p < 0.01$ by one-sample *t* test. The experiment was performed with three biological replicates.

mediated FIH1 knockout (KO) HEK293 cells (Fig. 2*A*) and expressed GFP-Cezanne in these cells in the absence and presence of exogenous FIH1. As additional control, Cezanne- and FIH1-expressing cells were treated with hypoxia (1% oxygen) for 16 h (Fig. 2*B*). Subsequently, GFP-Cezanne was immunoprecipitated using nano-traps, and peptides were generated by tryptic digest, separated by LC, and analyzed by tandem MS. Hydroxylation of Asn[35] (mass change of +16 Da in the corresponding peptide) was robustly detected in the presence of FIH1 and oxygen (Fig. 2, *C* and *D*). Under hypoxic conditions, when FIH1 activity was limited, or in the absence of FIH1 protein, hydroxylation of Asn[35] was significantly reduced. Depletion of FIH1 did not change Cezanne protein level, suggesting that expression or stability of Cezanne did not depend on hydroxylation (Fig. 2*A* and Fig. S1*A*). Moreover, there is no evidence that FIH1 is a substrate for Cezanne-mediated deubiquitination, at least Cezanne does not seem to remove proteolytic ubiquitin signals from FIH1, because Cezanne knockdown does not affect FIH1 protein level (9). In summary, our observations confirmed that the predicted FIH1 consensus site of Cezanne is recognized by the hydroxylase and that Cezanne is modified in an oxygen- and FIH1-dependent manner. Interestingly, the hydroxylated asparagine residue lies within the UBA domain of Cezanne, suggesting that asparagine hydroxylation, a PTM that has never been associated with a UBD before, may regulate the interaction between UBA$^{Cez}$ and ubiquitin.

### *Hydroxylation of Asn[35] affects UBA-ubiquitin binding*

Based on our finding that UBA$^{Cez}$ is hydroxylated, we investigated the properties of this domain and a potential regulation of ubiquitin binding by hydroxylation in more detail. At this point, we had no evidence that UBA$^{Cez}$ has a direct effect on the catalytic activity of Cezanne. *In vitro* DUB assays showed that

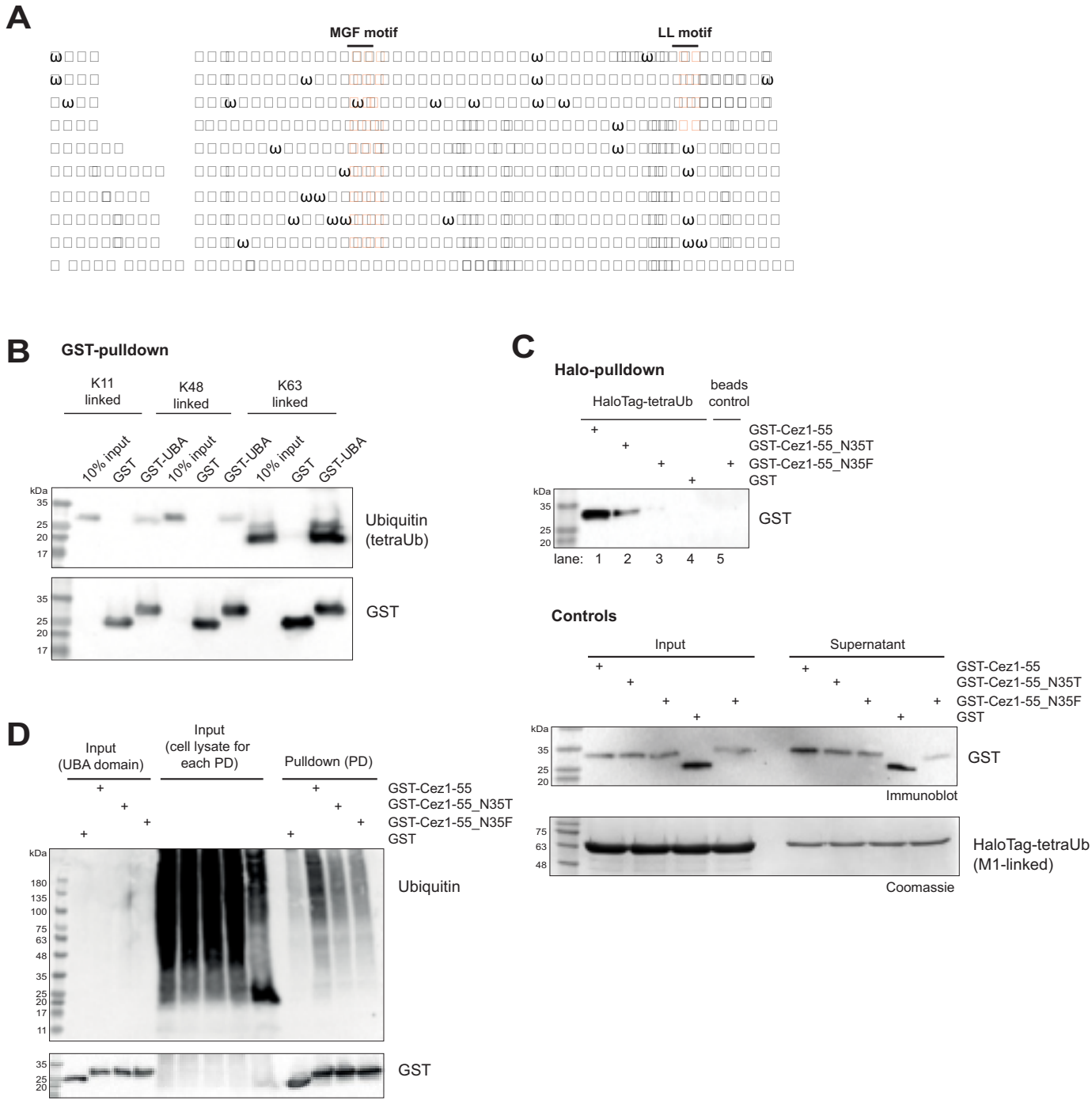


**Figure 3. Cezanne's UBA domain binds polyubiquitin of different linkage types.** *A*, sequence alignment of various UBA domains revealed that UBA$^{Cez}$ lacks both the MGF motif and the dileucine motif. *B*, Western blotting showing *in vitro* GST pulldown assay. GST-UBA$^{Cez}$ co-precipitated Lys$^{11}$-, Lys$^{48}$-, and Lys$^{63}$-linked tetraubiquitin. *C*, *in vitro* pulldown of WT and mutant UBA$^{Cez}$ and Halo-tagged tetraubiquitin (Met$^{1}$-linked). Mutation of Asn$^{35}$ in UBA$^{Cez}$ greatly reduced ubiquitin binding. *D*, semi-*in cellulo* pulldown of recombinant WT or mutant UBA$^{Cez}$ and ubiquitinated proteins from HEK293 cells treated with the proteasome inhibitor MG132.

the presence of UBA$^{Cez}$ did not alter the ability of Cezanne's catalytic OTU domain to cleave Lys$^{11}$-linked tetraubiquitin (Fig. S1*B*). Furthermore, the addition of FIH1 protein to the *in vitro* reaction did not affect the activity of Cezanne, excluding the possibility that interaction with FIH1 regulates Cezanne activity allosterically (Fig. S1*C*).

Sequence alignment of multiple UBA domains showed that UBA$^{Cez}$ contains neither the conserved MGF motif nor a dileucine motif (Fig. 3*A*), which form a hydrophobic surface patch and play an important role in ubiquitin recognition by other UBA domains (31). Also, it has never been shown *in vitro* that UBA$^{Cez}$ is a functional UBD and indeed binds ubiquitin. This is

more than a formality because, for example, the UBA domains of the E3 ubiquitin ligases Cbl-b and c-Cbl share a high sequence similarity, and both adopt the typical UBA fold, a compact three-helix bundle. However, only Cbl-b is able to efficiently interact with ubiquitin (14). We designed a human $UBA^{Cez}$ construct for recombinant expression based on the structure prediction provided by the Phyre2 server (32) (predicted UBA domain: residues 4–49) and performed *in vitro* pulldown experiments. Numerous UBA domains bind polyubiquitin in strong preference to monoubiquitin, and some of them selectively bind specific linkage type(s) (12, 33). To determine whether $UBA^{Cez}$ exhibits selectivity toward a certain ubiquitin linkage type, we compared the binding efficiency of $Lys^{11}$-, $Lys^{48}$-, and $Lys^{63}$-linked tetraubiquitin. $UBA^{Cez}$ co-precipitated all tested ubiquitin chain types in a GSH-*S*-transferase (GST) pulldown experiment, which confirmed the integrity of the UBD and its ability to bind polyubiquitin (Fig. 3*B*). Although our experiments suggested that $UBA^{Cez}$ binds $Lys^{63}$-linked ubiquitin chains slightly better than the other polyubiquitin chains (Fig. 3*B*), this observation is likely due to the dimeric GST tag that has been shown to position two UBA domains for avid interactions with $Lys^{63}$-linked polyubiquitin, but not other ubiquitin linkage types (33).

To investigate a potential impact of asparagine hydroxylation on the $UBA^{Cez}$-ubiquitin interaction, we first created different $UBA^{Cez}$ mutant constructs and analyzed their ability to bind tetraubiquitin. We focused on linear ($Met^1$-linked) ubiquitin chains because they are structurally very similar to $Lys^{63}$-linked polyubiquitin and readily bound $UBA^{Cez}$ (Fig. 3*C*, *lane 1*). In contrast to lysine-linked ubiquitin chains that are conjugated via isopeptide bonds and need to be enzymatically assembled, linear ubiquitin chains can be recombinantly expressed in large quantities and allowed us further biochemical and structural analyses. Mutation of $Asn^{35}$ to a threonine residue in $UBA^{Cez}$(N35T), which exhibits a hydroxyl group at its $\beta$-carbon similar to hydroxylated asparagine, resulted in less efficient binding to Halo-tagged tetraubiquitin as compared with the WT domain (Fig. 3*C*, *lane 2*), whereas mutation of $Asn^{35}$ to a bulky phenylalanine residue, $UBA^{Cez}$(N35F), almost completely abolished interaction with ubiquitin (Fig. 3*C*, *lane 3*). Moreover, GST-tagged $UBA^{Cez}$(N35T) and $UBA^{Cez}$(N35F) bound and immobilized less efficiently ubiquitinated proteins from HEK293 cell lysates treated with MG132 than did WT $UBA^{Cez}$ (Fig. 3*D*).

To further explore how asparagine hydroxylation impacts ubiquitin binding, we co-expressed FIH1 and GST-tagged $UBA^{Cez}$ in *Escherichia coli* and subsequently purified the recombinant, hydroxylated UBA domain (Fig. 4*A*). FIH1 was able to directly modify $UBA^{Cez}$ at $Asn^{35}$ within the bacterial cells. Hydroxylation of purified $UBA^{Cez}$ was confirmed by MS (Fig. 4*B*). Using a GST pulldown assay, we then compared binding efficiency of linear tetraubiquitin with unmodified and hydroxylated $UBA^{Cez}$, respectively. We revealed that hydroxylation of $UBA^{Cez}$ significantly reduced its interaction with tetraubiquitin (Fig. 4*C*), which confirmed the results obtained by using mutant $UBA^{Cez}$(N35T) and (N35F) (Fig. 3, *C* and *D*).

Together, our data show that $UBA^{Cez}$ binds differently linked ubiquitin chains independent of classic UBA features and that FIH1-mediated hydroxylation of $Asn^{35}$ impairs UBA domain-ubiquitin binding.

### *The UBA domain of Cezanne interacts with ubiquitin via a unique binding mode*

Our pulldown experiments suggested that $UBA^{Cez}$ binds ubiquitin in a noncanonical way because it lacks conserved domain properties. For further characterization of how $UBA^{Cez}$ interacts with ubiquitin, we performed NMR titration experiments in which nonlabeled UBA domain was titrated to $^{15}$N-labeled linear diubiquitin (Fig. 5, *A–D*). Binding of $UBA^{Cez}$ resulted in significant chemical shift perturbations (CSP) that were predominantly in the fast to intermediate exchange modes (Fig. 5*A* and Fig. S2). This corresponds to rather weak interactions between the two proteins, as typically observed for UBA domains ($K_D$ in the range of 100 $\mu$M) (12). Interestingly, one-third of residues in the spectra of linear diubiquitin showed double resonances in the free form (similar to the free linear diubiquitin NMR spectra presented previously (34)), indicating a conformational nonequality of the proximal and distal ubiquitin moieties. For many residues, this nonequality was enhanced upon interaction with $UBA^{Cez}$ (Fig. S2). To distinguish between CSP located on the distal and proximal ubiquitin, we first mapped all CSP on the distal ubiquitin moiety, filtered out all double peaks in the spectra from the CSP mapping, and transferred them onto the proximal ubiquitin moiety to create a resulting map of CSP on linear diubiquitin (Fig. S3).

CSP mapping on the linear diubiquitin three-dimensional structure (PDB code 2W9N (35)) revealed a rather specific interface that included residues of both the distal and proximal ubiquitin, as well as the linker region (Fig. 5*C*). However, the absolute orientation of the binding interface could not be sufficiently resolved due to various linear diubiquitin structures available that show different angles of the orientation of both ubiquitin moieties.

To determine the binding surface of linear diubiquitin on the $UBA^{Cez}$, we performed the reverse titration experiment in which nonlabeled diubiquitin was titrated to $^{15}$N-labeled $UBA^{Cez}$ (Fig. 5, *E–H*). Most residues of $UBA^{Cez}$ showed CSP in the fast exchange mode. However, some residues in the domain showed CSP in the intermediate exchange with significant resonances broadening and therefore a different dynamic behavior upon interaction with linear diubiquitin. CSP sequential mapping revealed that these residues are located at the C-terminal region of $UBA^{Cez}$ but also included $Leu^{22}$ (Fig. 5*F*). Because no structure of Cezanne's UBA domain was available, we modeled a structure using protein online tools (www.proteinmodelportal.org,[3] with NMR structure of human UBA-like domain of OTUD7A as a template) and mapped the calculated CSP on this model (Fig. 5*G* and Fig. S4). Surprisingly, the residues that are most affected by the interaction with linear diubiquitin were located around helices $\alpha$2 and $\alpha$3 of the $UBA^{Cez}$ and formed an extended hydrophobic area on the domain surface. Notably, $Asn^{35}$ exhibited no CSP upon the addition of linear diubiquitin (neither for

[3] Please note that the JBC is not responsible for the long-term archiving and maintenance of this site or any other third party hosted site.

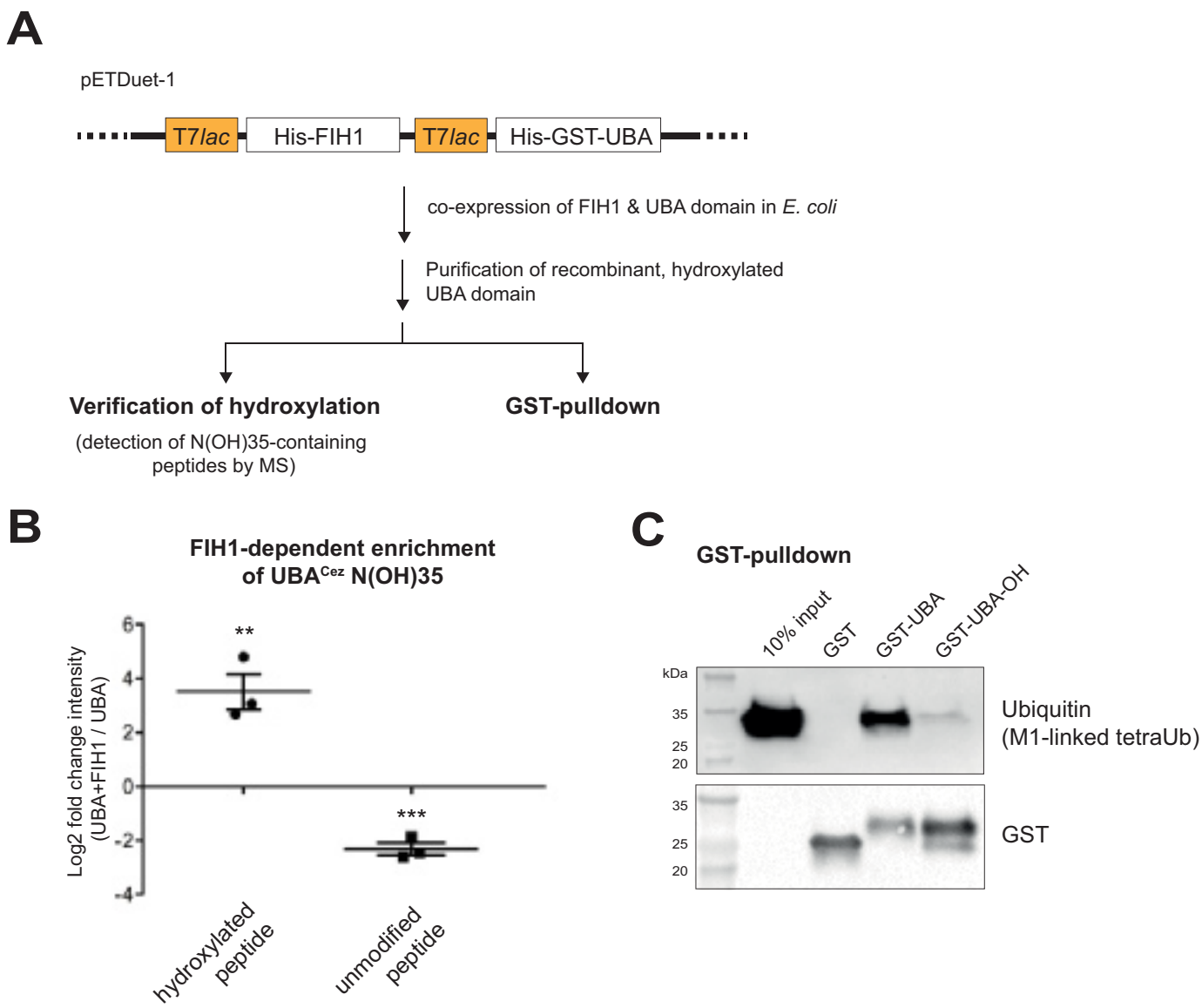


**Figure 4. Hydroxylation of Asn$^{35}$ modulates UBA-ubiquitin interaction.** *A, cartoon* depicting experimental strategy for assessing the effect of asparagine hydroxylation on ubiquitin binding. *B,* verification of FIH1-dependent enrichment of Asn$^{35}$ hydroxylation of recombinant UBA$^{Cez}$ by MS analysis. Data are represented as mean of $\log_2$-fold change intensity plus S.E. (*error bars*). **, $p < 0.01$; ***, $p < 0.001$ by one-sample *t* test. The experiment was performed with three biological replicates. *C, in vitro* GST pulldown assay comparing interaction of linear tetraubiquitin with unmodified and hydroxylated UBA$^{Cez}$, respectively.

backbone HN nor for side-chain $NH_2$ group). Our pulldown experiments showed that mutation or hydroxylation of Asn$^{35}$ affected ubiquitin binding (Figs. 3 (*C* and *D*) and 4*C*), indicating a potential conformational effect of these modifications, rather than an involvement in ubiquitin binding. Similar properties were observed for residues Ser$^{9}$ and Leu$^{10}$, which were previously suggested to be involved in UBA$^{Cez}$-ubiquitin interaction (6) but showed no or only minor CSP in our NMR titration experiments. The overall ubiquitin binding mode observed for UBA$^{Cez}$ differed significantly from other UBA domains. Most of the UBA-ubiquitin interactions studied so far indicate that ubiquitin is bound via helices $\alpha$1 and $\alpha$3 of UBA domains, and thus via a different surface than on UBA$^{Cez}$.

To understand whether ubiquitin polymerization affects the binding of UBA$^{Cez}$, we repeated the NMR experiments with monoubiquitin (Fig. S5). Monoubiquitin interacted with UBA$^{Cez}$ in a fast exchange mode, showing a lower affinity and absence of conformational uncertainties. Accordingly, some residues, such as Leu$^{8}$ or Ile$^{13}$, showed intermediate exchange behavior in linear diubiquitin and fast exchange mode in monoubiquitin upon binding to UBA$^{Cez}$ (Fig. S5, *A–D*). Similar changes were observed for the interaction mode in reciprocal titration ($^{15}$N-labeled UBA$^{Cez}$ was titrated with nonlabeled linear di- or monoubiquitin). Whereas CSP for interaction between UBA$^{Cez}$ and linear diubiquitin were in the fast to intermediate exchange mode, the binding of monoubiquitin resulted in a fast exchange mode exclusively (Fig. S5, *E–H*). Additionally, some residues of UBA$^{Cez}$ showed a different CSP pattern (*e.g.* Ala$^{7}$ and Leu$^{22}$; Fig. S5, *E* and *G*) upon binding of either linear di- or monoubiquitin, indicating not only a difference in the binding modes, but also involvement of these residues in the specific recognition of ubiquitin chains.

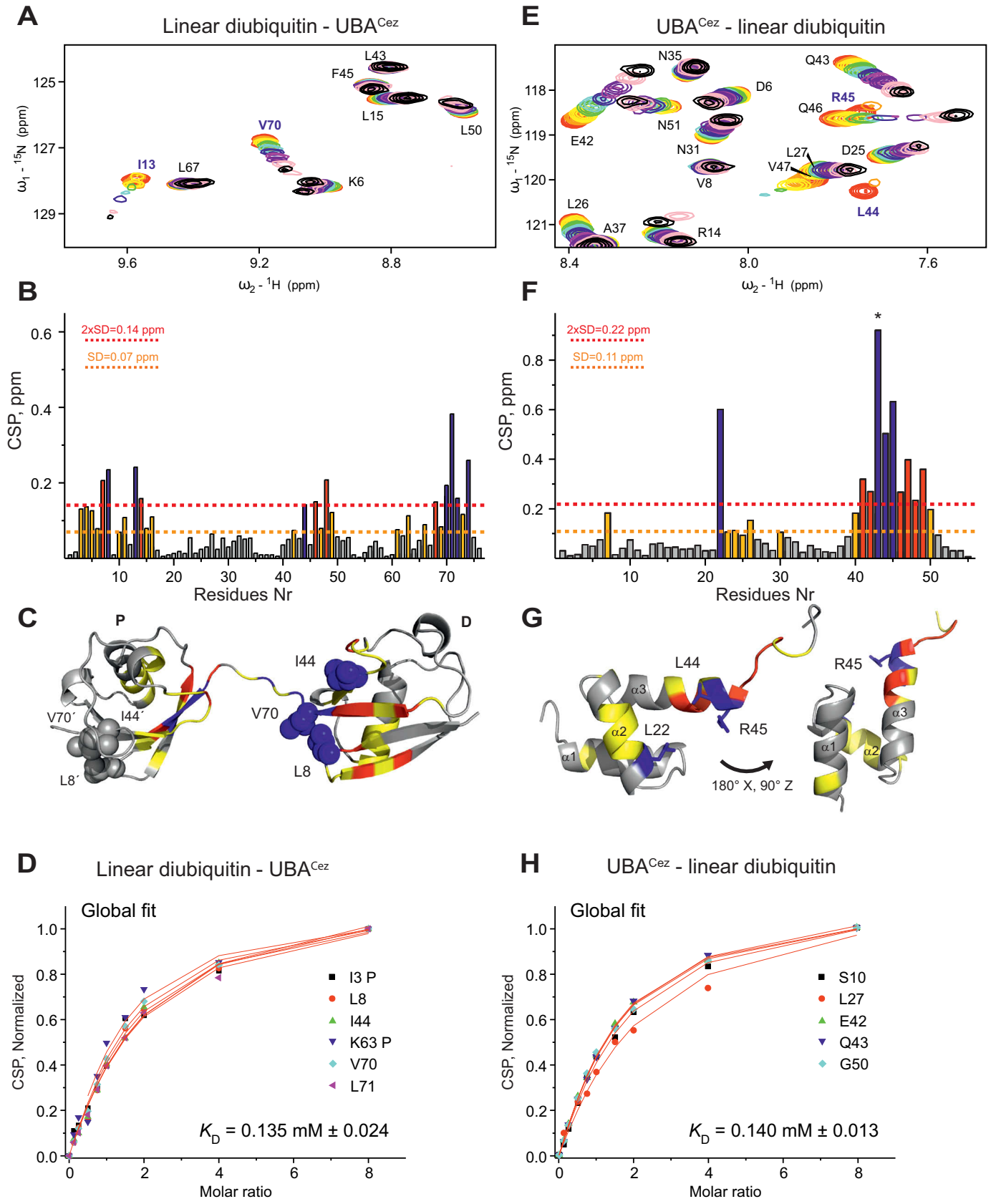
A
Linear diubiquitin - UBA^Cez
L43
F45
L15
L50
V70
I13
L67
K6
125
127
129
ω1 - 15N (ppm)
9.6
9.2
8.8
ω2 - 1H (ppm)
E
UBA^Cez - linear diubiquitin
N35
Q43
D6
R45
Q46
N51
E42
N31
L27
D25
V47
V8
L44
L26
A37
R14
118
119
120
121
8.4
8.0
7.6
B
2xSD=0.14 ppm
SD=0.07 ppm
CSP, ppm
0.6
0.4
0.2
10
20
30
40
50
60
70
Residues Nr
F
2xSD=0.22 ppm
SD=0.11 ppm
*
0.8
C
P
D
I44
V70
V70´
I44´
L8´
L8
G
L44
R45
α3
α2
L22
α1
180° X, 90° Z
D
Linear diubiquitin - UBA^Cez
Global fit
CSP, Normalized
I3 P
L8
I44
K63 P
V70
L71
K_D = 0.135 mM ± 0.024
Molar ratio
H
UBA^Cez - linear diubiquitin
Global fit
S10
L27
E42
Q43
G50
K_D = 0.140 mM ± 0.013
Molar ratio

Based on the NMR titration experiments, we calculated $K_D$ values for six residues of linear diubiquitin and UBA$^{Cez}$ upon their interaction, respectively (Fig. 5 (*D* and *H*) and Fig. S6). In both cases, global fit for all residues showed $K_D$ values of ~0.14 mM and was therefore in agreement with reported affinities for other UBA domains and ubiquitin. Calculated $K_D$ values for the same residues in the case of interaction between UBA$^{Cez}$ and monoubiquitin resulted in values between 0.26 and 0.32 mM, which are 2-fold higher than for diubiquitin (Fig. S6, *A–D*), indicating that ubiquitin chain polymerization does not enhance the binding affinities dramatically.

To investigate the impact of FIH1-dependent hydroxylation of UBA$^{Cez}$ on its capacity to bind ubiquitin, we recorded NMR spectra of the $^{15}$N-labeled hydroxylated form of UBA$^{Cez}$ (Asn$^{35}$OH) and mutant UBA$^{Cez}$ (N35T). Our data confirmed that neither hydroxylation nor mutation of Asn$^{35}$ in UBA$^{Cez}$ interferes with the overall fold of the protein (Fig. S7). However, comparison of the NMR spectra of modified and WT UBA$^{Cez}$ revealed that the changes in resonance position are not limited to the closest Asn$^{35}$ neighborhood but extended to a number of residues located N- and C-terminally to Asn$^{35}$ (Fig. S7, *A–C*). This fact suggests that Asn$^{35}$ modification affects the local structure and/or dynamics of residues in these areas and could influence binding of ubiquitin. Indeed, NMR titration experiments for UBA$^{Cez}$ with hydroxylated and mutated Asn$^{35}$ showed their reduced affinity to monoubiquitin (Fig. S7, *D* and *E*).

In summary, our NMR analyses reveal that UBA$^{Cez}$ physically interacts with monoubiquitin and linear polyubiquitin in the absence of the well-characterized MGF motif via a noncanonical binding surface involving helices α2 and α3 of the UBA domain and that Ala$^{7}$ and Leu$^{22}$ in UBA$^{Cez}$ seem to participate in specific recognition of linear ubiquitin chains. However, dimerization of two ubiquitin molecules does not enhance UBA$^{Cez}$ affinity to the monoubiquitin moiety. Furthermore, Asn$^{35}$ is not involved in direct contacts to ubiquitin; its hydroxylation rather changes the local structure and/or dynamics of UBA$^{Cez}$ regions that contact ubiquitin directly. These changes reduce the affinity of UBA$^{Cez}$ to monoubiquitin.

## Discussion

Different layers of DUB regulation have been described to ensure proper enzymatic function. PTMs, regulatory domains within DUBs, and the incorporation of DUBs into macromolecular complexes are means of both temporal and spatial control. In addition to its catalytic OTU domain, Cezanne comprises two UBDs and a nuclear localization signal, which have been suggested to regulate Cezanne's cellular localization and its recruitment to substrates (5, 6, 36). Furthermore, several phosphorylation sites within Cezanne have been described (37); their functions, however, remain elusive.

Here, we identify Cezanne as novel substrate for the asparaginyl β-hydroxylase FIH1 and determine that Cezanne is posttranslationally hydroxylated at Asn$^{35}$ within its UBA domain in an oxygen- and FIH1-dependent manner. We demonstrate that UBA$^{Cez}$ nonselectively binds Lys$^{11}$-, Lys$^{48}$-, Lys$^{63}$-, and Met$^{1}$-linked (linear) ubiquitin chains *in vitro*, although it lacks the classic hydrophobic ubiquitin interaction motifs described in other UBA domains. Importantly, hydroxylation of Asn$^{35}$ inhibits ubiquitin binding by UBA$^{Cez}$. Our study is the first one implicating asparagine hydroxylation in the regulation of UBA domain-ubiquitin interactions.

Cezanne has been associated with multiple cellular pathways, most recently with the regulation of mitotic progression (11). Although the catalytic OTU domain of Cezanne selectively hydrolyzes Lys$^{11}$-linked ubiquitin chains *in vitro*, various studies reported a Cezanne-dependent abundance of several ubiquitin linkage types *in vivo* (8, 10). One possible explanation for this discrepancy could be proximity effects, meaning that an acute increase in local concentration of Cezanne at its substrates in response to respective stimuli could allow the DUB to hydrolyze linkage types other than Lys$^{11}$ as well. The effect of proximity consists predominantly in increasing the effective concentration of the reactants and thereby increasing the reaction kinetics and allowing reactions that would not yield products in the absence of the concentration effect (38). In accordance with this model, Cezanne readily cleaves Lys$^{63}$-linked ubiquitin chains *in vitro* at higher enzyme concentrations (Fig. S1*D*). The two UBDs located at the N and C terminus of Cezanne could further promote an increase in Cezanne concentra-

**Figure 5. Binding between linear diubiquitin and the UBA domain of Cezanne.** Shown are the results for NMR titrations of $^{15}$N-labeled linear diubiquitin with nonlabeled UBA$^{Cez}$ (*A–D*) and NMR titrations of $^{15}$N-labeled UBA$^{Cez}$ with nonlabeled linear diubiquitin (*E–H*). *A*, representative area of $^{15}$N,$^{1}$H BEST-TROSY HSQC spectra for linear diubiquitin, to which UBA$^{Cez}$ was added in a specified molar ratio (1:8, 1:4, 1:2, 1, 2, 4, and 8), is shown. The *rainbow color code* indicates increased molar ratios upon titration from free linear diubiquitin (*red*) to full saturation upon 8-fold excess of UBA$^{Cez}$ (*dark gray*). *B*, CSP mapping on the ubiquitin sequence. *Yellow* and *red lines* indicate the 1× and 2× S.D. (δ) calculated from CSP values of all residues, respectively. Residues of linear diubiquitin, which showed double peaks (either in the free or UBA$^{Cez}$-bound form) and significant line broadening, are *colored* in *blue*. *C*, CSP mapping on the linear diubiquitin structure (PDB code 2L2D). The diubiquitin is presented as a *ribbon diagram*; *P* and *D symbols* indicate proximal and distal ubiquitin moieties. Residues with intermediately (δ ≤ CSP ≤ 2×δ) and strongly (CSP ≥ 2×δ) perturbed backbone HN resonances are marked in *yellow* and *red*, respectively. Residues with anomalous exchange behavior (described above) are marked in *blue*. Side chains of residues from the ubiquitin hydrophobic patch (Leu$^{8}$-Ile$^{44}$-Val$^{70}$) are shown as *spherical* atom models. *D*, $K_D$ calculated for the selected linear diubiquitin residues upon titration with UBA$^{Cez}$. Normalized CSP values of residues I3p (where p represents proximal ubiquitin), Leu$^{8}$, Ile$^{44}$, Lys$^{63}$p, Val$^{70}$, and Leu$^{71}$, showing significant CSP in the fast exchange mode, were used in the global fit. *E*, representative area of $^{15}$N,$^{1}$H BEST-TROSY HSQC spectra for UBA$^{Cez}$, to which linear diubiquitin was added in the specified molar ratio (1:8, 1:4, 1:2, 1, 2, 4, and 8), is shown. The *rainbow color code* indicates increased molar ratios upon titration from the free UBA$^{Cez}$ (*red*) to full saturation upon 8-fold excess of linear diubiquitin (*dark gray*). *F*, CSP mapping on the UBA$^{Cez}$ sequence. *Yellow* and *red lines*, 1× and 2× S.D. (δ) calculated from CSP values of all residues, respectively. Residues of UBA$^{Cez}$, which showed intermediate exchange and significant line broadening, are *colored* in *blue*. *, CSP for the side chain of Gln$^{43}$, which shows intermediate and big CSP upon binding of linear diubiquitin. *G*, CSP mapping on the modeled UBA$^{Cez}$ structure. The UBA$^{Cez}$ is presented as a *ribbon diagram*. Residues with intermediately (δ ≤ CSP ≤ 2×δ) and strongly (CSP ≥ 2×δ) perturbed backbone HN resonances are marked in *yellow* and *red*, respectively. Residues with anomalous exchange behavior (described above) are marked in *blue*. *H*, $K_D$ calculated for the selected UBA$^{Cez}$ residues upon titration with linear diubiquitin. Normalized CSP values of residues Ser$^{10}$, Leu$^{27}$, Glu$^{42}$, Gln$^{43}$, and Gly$^{50}$, showing significant CSP in the fast exchange mode, were used in the global fit.

tion at its substrates by additionally binding polyubiquitin attached to substrates and/or other proteins that are in complex with Cezanne substrates. Consistent with this, it has been shown that Cezanne deubiquitinates EGFR and thereby inhibits the ligand-dependent degradation of the receptor and that the A20-like ZnF of Cezanne is essential for this effect (5). In contrast to $UBA^{Cez}$, which binds ubiquitin via the classic $Ile^{44}$ patch of ubiquitin (Fig. 5*B*), Cezanne's ZnF interacts with the ubiquitin surface centered on $Asp^{58}$. In the absence of the ZnF, Cezanne failed to inhibit EGFR degradation. In addition, it has been suggested that Cezanne is recruited to the activated TNFR complex via $UBA^{Cez}$, where it binds $Lys^{63}$-linked ubiquitin chains and exerts its function as a negative regulator of NF-κB activation (6). Our *in vitro* studies confirm the ability of $UBA^{Cez}$ to bind $Lys^{63}$-linked polyubiquitin and also show that $UBA^{Cez}$ interacts with $Lys^{11}$-, $Lys^{48}$-, and $Met^{1}$-linked ubiquitin chains. Recruitment of Cezanne to and accumulation at substrates modified with ubiquitin linkage types other than $Lys^{11}$ thus appears feasible. Alternatively, Cezanne could serve to preclude unwanted assembly of $Lys^{11}$-linked ubiquitin chains on these proteins. Furthermore, hydroxylation of $UBA^{Cez}$, which impairs the ability of the domain to bind ubiquitin, could prevent nonspecific accumulation of Cezanne at ubiquitinated substrates and interacting proteins.

FIH1-dependent asparagine hydroxylation is more abundant than originally anticipated. In addition to the transcription factor HIF1α, multiple other FIH1 substrates have been identified in the last decade. Asparagine hydroxylation mainly regulates protein-protein interactions. In the case of Cezanne, this PTM is located within its UBA domain, namely at $Asn^{35}$. To understand the function of hydroxylation in the context of $UBA^{Cez}$, we mutated $Asn^{35}$ in an attempt to mimic hydroxylation or rather to introduce spatial constraints for ubiquitin binding and observed that both threonine and phenylalanine residues at position 35 significantly reduce the interaction with ubiquitin in pulldown experiments, just as hydroxylation of $Asn^{35}$ did. Interestingly, our NMR data imply that $Asn^{35}$ is not part of the $UBA^{Cez}$ surface that is recognized by ubiquitin, which suggests that asparagine hydroxylation, or threonine and phenylalanine residues at position 35 within the UBA domain, probably affect the structural integrity of the domain. It has been proposed that asparagine residues are preferentially located at the N-cap position of α-helices, and our predicted structure of $UBA^{Cez}$ positions $Asn^{35}$ within this area. The N-cap residue is the first amino acid whose α-carbon lies approximately in the cylinder formed by the helix backbone and approximately along the helical spiral path. It is the first residue (I) whose CO group is hydrogen-bonded to the HN group of residue I+4 (or sometimes I+3; therefore it can also be described as the residue prior to the helix). In addition, the δ-oxygen of asparagine residues can form a hydrogen bond to the backbone NH group of residue $Asn^{3}$ (or sometimes $Asn^{2}$) exposed in the first turn of the helix (39). It has been suggested that asparagine residues could help to specify the location of the helix N terminus, because it can simultaneously stabilize the first helical turn by providing an additional interaction equal to that of a residue and also discourage further helix propagation in the N-terminal direction by competing with the backbone to provide that interaction (39). It is thus likely that mutation of $Asn^{35}$, or changing polarity of the asparagine side chain by hydroxylation of the β-carbon, can change the spatial organization of helix α3 relative to the other helices. Because $UBA^{Cez}$ specifically engages ubiquitin via a surface comprising helices α2 and α3, hydroxylation of $Asn^{35}$ could therefore affect ubiquitin binding, although it is not part of the direct interacting surface. Consistently, we observed by NMR titration experiments that hydroxylation of $Asn^{35}$ or its mutation reduces the affinity of $UBA^{Cez}$ to monoubiquitin. Furthermore, the observed differences in NMR spectra of $UBA^{Cez}(Asn^{35}OH)$ and $UBA^{Cez}(N35T)$ compared with that of the WT domain confirm our hypothesis that hydroxylation of $Asn^{35}$, a residue not part of the $UBA^{Cez}$-ubiquitin binding interface, affects the conformation and/or dynamics of $UBA^{Cez}$ regions directly participating in ubiquitin recognition. Although calculated $K_D$ values of the $UBA^{Cez}$-monoubiquitin interaction only moderately increased upon $Asn^{35}$ hydroxylation, we hypothesize that the observed drop in affinity for ubiquitin will be even more pronounced with increasing numbers of conjugated ubiquitin moieties in the chain as observed in our pulldown experiments using tetraubiquitin (Fig. 4*C*).

Interestingly, within the UBA domain of OTUD7A (Cezanne 2), Cezanne's closest but rather unstudied relative, there is a threonine residue at the corresponding position for $Asn^{35}$ (*i.e.* $Thr^{57}$). The UBA domain is highly conserved between Cezanne and OTUD7A. Our pulldown assays showed that a threonine residue at this position within the UBA domain strongly reduced interaction with ubiquitin. Therefore, it can be assumed that $UBA^{OTUD7A}$ binds ubiquitin less efficiently than $UBA^{Cez}$ and that the UBA domain may not contribute to OTUD7A recruitment to substrates and interacting proteins in the same way as $UBA^{Cez}$.

Furthermore, our group has shown that Cezanne plays an important role for proper HIF target gene expression in hypoxic condition by stabilizing HIF1α (9). FIH1 has a high affinity for oxygen and remains partially functional in hypoxia. An additional purpose for Cezanne hydroxylation in the context of HIF1α regulation could be to sequester FIH1, thereby reducing HIF1α CTAD hydroxylation and further promoting HIF activity.

## Experimental procedures

### *Cell culture and transfection*

HEK293 and 293T cells were obtained from Leibnitz Institute DSMZ-German Collection of Microorganisms and Cell Culture (DSMZ nos. ACC 305 and ACC 635, respectively) and grown in DMEM–GlutaMAX™-I medium (Gibco/Life Technologies) supplemented with 10% (v/v) fetal bovine serum (Gibco/Life Technologies) and 50 units/ml penicillin and 50 μg/ml streptomycin (GE Healthcare) at 37 °C and 5% $CO_2$. PCR-based *Mycoplasma* contamination tests were regularly performed using the Venor®GeM Classic kit (Minerva Biolabs). Hypoxia treatment at 1% oxygen was achieved using a Whitley H35 Hypoxystation (Meintrup DWS Laborgeräte). To avoid reoxygenation, cells were lysed in the hypoxia chamber. For immunoblotting, $1 \times 10^6$ cells/well were seeded in 6-well plates and transfected after 24 h with 1–3 μg of DNA using polyeth-

yleneimine, 25 kDa, linear (PEI) (Polysciences Europe). For 1 $\mu$g of DNA, 3 $\mu$l of PEI (1 mg/ml) and 200 $\mu$l of prewarmed Opti-MEM medium (Gibco/Life Technologies) were used. After transfection, cells were cultured for 24 h prior to lysis.

### *Co-immunoprecipitation*

$1 \times 10^6$ HEK293 cell/well were seeded in 6-well plates and transfected after 24 h. GFP-tagged Cezanne constructs were co-expressed with untagged FIH1 (WT or mutants) for 24 h. Cells were washed with PBS and lysed on ice for 10 min (10 mM Tris-HCl (pH 7.5), 150 mM NaCl, 1% Triton X-100, 1 × cOmplete, EDTA-free protease inhibitors (Roche Applied Science), 100 mM PMSF, 100 mM NaF). Cell debris was removed by centrifugation at 15,000 × *g* for 10 min at 4 °C. Per sample, 2–3 wells of a 6-well plate were transfected and combined after lysis. 10% of clarified lysate was taken as the input sample and mixed with 4× LDS sample buffer (Invitrogen/Life Technologies) supplemented with 20 mM DTT. 10 $\mu$l of GFP-Trap® agarose slurry (Chromotek)/well of a 6-well plate were mixed with the clarified lysate and incubated on a rotary shaker for 1 h at 4 °C. The beads were washed five times with wash buffer (10 mM Tris-HCl (pH 7.5), 150 mM NaCl, 1× cOmplete, EDTA-free protease inhibitors (Roche Applied Science)). Immobilized proteins were eluted with 40 $\mu$l of 2× LDS sample buffer (Invitrogen/Life Technologies) supplemented with 20 mM DTT. 20 $\mu$l of IP sample and 15 $\mu$l of input sample were analyzed by SDS-PAGE and immunoblotting.

### *Immunoblotting*

Proteins were separated on precast Mini-PROTEAN TGX gradient gels (4–15% or 4–20%, Bio-Rad) or self-made Tris-glycine gels and transferred (200 mA for 90 min) onto 0.45-$\mu$m Immobilon-IP polyvinylidene fluoride membranes (Millipore) or 0.45-$\mu$m nitrocellulose membranes (Millipore) using the Mini Trans-Blot Cell System (Bio-Rad). Protein Marker VI (10–245 kDa) prestained (AppliChem) was used as a protein marker. Membranes were blocked with 5% milk in TBST (50 mM Tris-HCl (pH 7.6), 150 mM NaCl, 0.05% Tween® 20). Blots were incubated overnight at 4 °C with primary antibodies. Blots were washed three times (each 5 min) with TBST and incubated for 1 h at room temperature with secondary antibodies (HRP-conjugated for chemiluminescence). Subsequently, blots were washed twice with TBST and once with TBS (50 mM Tris-HCl (pH 7.6), 150 mM NaCl). For chemiluminescence visualization, blots were incubated with ECL Prime Western blotting detection reagent (GE Healthcare) and detected with the Chemi-Doc™ Imaging System (Bio-Rad).

### *Antibodies*

The following antibodies at the indicated concentrations were used in this study: mouse anti-GFP (B-2) (Santa Cruz Biotechnology, Inc., sc-9996, 1:2000), rabbit anti-FIH (Novus, NB100-428, 1:2000), rabbit anti-OTUD7B/Cezanne (Cell Signaling, 14817, 1:2000), rabbit anti-ubiquitin (Cell Signaling, 3933, 1:2000), rabbit anti-GST (91G1) (Cell Signaling, 2625P, 1:2000). Secondary antibodies used in this study were obtained from Santa Cruz Biotechnology: anti-mouse IgG-HRP (sc-2096, 1:10,000) and anti-rabbit IgG-HRP (sc-2054, 1:10,000). All primary antibodies were diluted in 3% BSA (prepared in TBST, 0.05% Tween® 20, and 0.05% sodium azide). Secondary antibodies were diluted in 5% nonfat dried milk (prepared in TBST).

### *Cloning and site-directed mutagenesis*

Oligonucleotide primers were designed with the In-Fusion Cloning Primer Design Tool (Clontech) and purchased from Sigma-Aldrich. FLAG-HA-OTUD7B (a gift from Wade Harper, Addgene plasmid 22550) was used as template to amplify Cezanne/OTUD7B (full-length and truncated versions) for cloning into pEGFP-N1 mammalian expression vector and pOPINK or pETDuet-1 bacterial expression vector using the In-Fusion cloning system (In-Fusion®HD Cloning Kit, Clontech) according to the manufacturer's instructions. pcDNA3-FIH1 was a gift from Eric Metzen (Addgene plasmid 21399). Linear diubiquitin was purchased as an *E. coli* codon-optimized DNA sequence (GenScript) that was cloned into the NdeI and BamHI sites present in pET39 bacterial expression vector using T4 DNA ligase (New England Biolabs). The resulting linear diubiquitin construct included an N-terminal $His_{10}$ tag followed by a tobacco etch virus cleavage site.

Site-directed mutagenesis of Cezanne and FIH1 was performed using the QuikChange method. A 50-$\mu$l reaction mix containing 40 ng of template DNA, 1× Phusion HF buffer (New England Biolabs), 1 mM dNTPs, 10 pmol of forward and reverse primers containing the desired mutation(s), 3% DMSO, 0.5 $\mu$l (1 unit) of Phusion High-Fidelity DNA polymerase (New England Biolabs), and autoclaved Milli-Q water was subjected to PCR using the following program: 98 °C for 2 min, (98 °C for 30 s; 55 °C for 20 s; 72 °C for 1 min/kb) × 35 cycles; 72 °C for 10 min, and 4 °C until further processing. The PCR was incubated with 2 $\mu$l of DpnI (New England Biolabs) for 2 h at 37 °C, and the amplified plasmid was purified using the QIAQuick gel extraction kit (Qiagen). Stellar™ competent cells (Clontech) were transformed using the purified plasmid. Successful mutation was verified by SANGER sequencing (Microsynth SeqLab).

### *Guide RNA design and CRISPR/Cas9 plasmid generation*

FIH1 knockout HEK293 cells were generated using the CRISPR-Cas9 technology. Guide RNA sequences targeting spCas9 to the genomic locus of FIH1 (ID Ensemble ENSG00000166135) were designed according to Ref. 40. Specific overhangs for subsequent ligation into pLenti-CRISPRv2 (gift from Feng Zhang, Addgene plasmid 52961) were added to each guide (underlined): HIF1AN_KO-1-F, CACCGaactggattaataagcaaca; HIF1AN_KO-1-R, AAACtgttgcttattaatccagttC; HIF1AN_KO-2-F, CACCGaggcactcgaactgatccgg; HIF1AN_KO-2-R, AAACccggatcagttcgagtgcctC; HIF1AN_KO-3-F, CACCGcaaacgctcaatgacactgt; HIF1AN_KO-3-R, AAACacagtgtcattgagcgtttgC.

Complementary oligonucleotides were annealed for 5 min at 95 °C and subsequently cooled down for 15 min at room temperature. Annealed primers were diluted to 0.5 $\mu$M in nuclease-free water and cloned into pLentiCRISPRv2 via BsmBI restriction enzyme (New England Biolabs) digest and subsequent ligation with T4 DNA ligase (New England Biolabs). Stellar™ competent cells (Clontech) were transformed with the ligation

reaction, and correct clones were identified by SANGER sequencing (Microsynth SeqLab) using the U6 primer.

### *Generation of high-titer lentivirus and viral transduction*

$7.5 \times 10^5$ HEK293T cells were seeded into a 6-well plate and cultivated in DMEM without antibiotics 24 h prior to transfection. Cells were transfected with Lipofectamine 2000 (Invitrogen/Life Technologies) by mixing the reagent with 200 $\mu$l of Opti-MEM and 3.3 $\mu$g of transfer vector containing the gRNAs (pLentiCRISPRv2), 2.7 $\mu$g of PAX2 (a gift from Didier Trono, Addgene plasmid 12260), and 1 $\mu$g of pMD2.G (a gift from Didier Trono, Addgene plasmid 12259). The transfection mix was incubated for 30 min at room temperature and afterward dropwise added to HEK293T cells. Medium was replaced with fresh DMEM containing 10% (v/v) fetal bovine serum (Gibco/Life Technologies) and 50 units/ml penicillin and 50 $\mu$g/ml streptomycin (GE Healthcare) 12 h after transfection. Supernatant containing lentiviral particles was collected after 24 and 48 h. Supernatants were pooled and frozen at −80 °C.

For viral transduction, supernatants have been thawed at room temperature, sterile-filtered through 0.45-$\mu$m filters, and mixed with 10 $\mu$g of Polybrene (Sigma-Aldrich) to infect $1 \times 10^6$ HEK293 cells. Stable transduced cells were selected with puromycin, and the efficiency of FIH1 knockout was confirmed by immunoblotting using antibody against FIH1.

### *Protein expression and purification*

All proteins were expressed in Rosetta™ (DE3) competent cells (Novagen). Respective cultures were grown at 37 °C until $A_{600}$ of 0.6 was reached. Protein expression was induced with 0.2–0.5 mM isopropyl $\beta$-D-thiogalactopyranoside (IPTG) overnight at 25 °C. Bacterial cultures were harvested by centrifugation and flash-frozen in liquid nitrogen. Bacterial pellets were thawed and cells were lysed by using a French press (Therma Electron). Lysis buffer for purification via His tag contained 500 mM sodium chloride, 50 mM sodium phosphate, 1 mg/ml lysozyme, 1 mg/ml DNase, 100 mM PMSF, 5 mM imidazole, 1× cOmplete, EDTA-free protease inhibitors (Roche Applied Science). Lysis buffer for purification via GST tag contained 270 mM sucrose, 50 mM Tris-HCl, 1 mg/ml lysozyme, 1 mg/ml DNase, 100 mM PMSF, 1× cOmplete, EDTA-free protease inhibitors (Roche Applied Science). Cell lysates were cleared by centrifugation and filtered through a 0.45-$\mu$m syringe filter. The supernatant was either applied onto a 5-ml HiTrap™ TALON® crude column (GE Healthcare) using the ÄKTA Pure 25 system or transferred into a glass chromatography column containing equilibrated GSH Sepharose™ 4B (GE Healthcare). For site-specific cleavage of the GST tag, immobilized fusion proteins were incubated with 30 mM PreScission protease (GE Healthcare) at 4 °C for 16 h. For purification of GST-tagged proteins, immobilized fusion proteins were eluted from GSH Sepharose™ 4B (25 mM Tris (pH 8.0), 150 mM NaCl, 25 mM GSH reduced). Proteins were further purified using a Superdex™ 75 10/300 GL size-exclusion chromatography column (GE Healthcare) equilibrated in 25 mM Tris-HCl (pH 7.5), 150 mM NaCl. Purified proteins were concentrated using Amicon® Ultra-4 concentrators (Millipore).

For NMR experiments, proteins were expressed in Luria–Bertani or M9 medium containing the $^{15}$N-labeled $NH_4Cl$ and $^{13}$C-labeled glucose. For expression of the UBA domain, Rosetta™ (DE3) competent cells (Novagen) were transformed with pOPINK-Cezanne (residues 1–55). Protein expression was induced with 0.25 mM IPTG for 12 h at 25 °C. For monoubiquitin and linear diubiquitin expression, T7 Express cells (New England Biolabs) were transformed with corresponding pET39 plasmids, induced with 0.2 mM IPTG, and harvested after 4 h of incubation at 37 °C. Monoubiquitin and linear diubiquitin were purified according to previous work (41). Protein samples were equilibrated in buffer containing 25 mM HEPES (pH 7.5), 50 mM NaCl, 5% $D_2O$ prior to NMR experiments.

### *Pulldown (PD) assays*

For GST pulldown experiments, equal amounts of GST and GST-tagged UBA domain were immobilized on GSH Sepharose™ 4B (GE Healthcare). After incubation for 1 h at 4 °C on a rotary shaker, beads were washed two times with PD buffer (150 mM NaCl, 50 mM Tris (pH 7.5), 5 mM DTT, 0.1% Nonidet P-40). Subsequently, 3 $\mu$g of differently linked tetraubiquitin chains were applied to coupled GST or GST-UBA beads in PD buffer containing 0.5 $\mu$g of BSA. Ubiquitin chains were incubated overnight at 4 °C on a rotary shaker. The next day, beads were washed five times with PD buffer and eluted with 4× LDS sample buffer (Invitrogen) supplemented with 20 mM DTT and boiled for 2 min at 95 °C.

For semi-*in cellulo* experiments, equal amounts of GST and GST-tagged UBA domain were immobilized on GSH beads. After incubation for 1 h at 4 °C on a rotary shaker, beads were washed two times with PD buffer (150 mM NaCl, 50 mM Tris (pH 7.5), 5 mM DTT, 0.1% Nonidet P-40). Subsequently, cell lysate from 293 cells (three wells of a 6-well plate were combined) treated for 2 h with 20 $\mu$M MG132 was applied to coupled GST and coupled GST-UBA beads and incubated for 2 h on a rotary shaker at 4 °C. Beads were washed five times with PD buffer and eluted with 4× LDS sample buffer (Invitrogen) supplemented with 20 mM DTT and boiled for 2 min at 95 °C.

For HaloTag pulldown experiments, 100 $\mu$l of HaloTag bead (Promega) suspension was incubated with 300 $\mu$g of Halo-tagged protein (Halo-linear tetraubiquitin or HaloTag alone) in Halo resin buffer (150 mM NaCl, 100 mM Tris (pH 7.5), 0.05% Nonidet P-40) at 4 °C for 1 h at room temperature. Input (before incubation) and supernatant (after incubation) samples were analyzed with SDS-PAGE followed by Instant Blue (Expedeon) staining to analyze whether beads were equally saturated with Halo-tagged protein. Beads were washed three times with Halo resin buffer. 2.5 $\mu$g of GST or GST-UBA protein were incubated for 1 h at 4 °C on a rotary shaker with immobilized Halo-protein. Afterward, beads were washed three times with Halo resin buffer and spun down at 800 × *g* for 5 min. Proteins were eluted with 2× LDS sample buffer (Invitrogen) supplemented with 20 mM DTT and boiled for 5 min at 95 °C.

### *In vitro Cezanne DUB assay*

Cezanne(1–449) or Cezanne(129–449) was diluted in 10 $\mu$l of DUB dilution buffer (25 mM Tris-HCl (pH 7.5), 150 mM NaCl, 10 mM DTT) and preincubated for 10 min at room

temperature. 1 $\mu$g of differently linked tetraubiquitin chains or diubiquitin was prepared in 10 $\mu$l of 10× DUB reaction buffer (500 mM Tris-HCl (pH 7.5), 500 mM NaCl, 50 mM DTT). To start the hydrolysis reaction, DUB and substrate were mixed in a 1:1 ratio and incubated at 37 °C for the indicated times. Reactions were stopped by adding 4× LDS sample buffer (Invitrogen/Life Technologies) supplemented with 20 mM DTT and boiled for 30 s at 95 °C. Samples were analyzed by SDS-PAGE on 4–20% gradient precast or 15% self-made gels and visualized by silver staining (Silver Stain Plus Kit, Bio-Rad).

### *NMR spectroscopy*

All NMR experiments were performed on Bruker Avance spectrometers operating at proton Larmor frequencies of 500 and 700 MHz at 25 °C and were analyzed using the Sparky 3.114 software (University of California, San Francisco). Backbone $^{1}$H and $^{15}$N resonances of the UBA domain of Cezanne were assigned using a $^{15}$N,$^{1}$H BEST-TROSY version of three-dimensional HNCACB (42) experiments with 0.8 mM uniformly $^{13}$C,$^{15}$N-labeled protein sample. Assignment of linear diubiquitin $^{1}$H and $^{15}$N resonances was taken from previously published work (34) (BMRB entry ID 26709) with minor adaptations. For NMR titration experiments, nonlabeled linear diubiquitin, monoubiquitin, or UBA domain was titrated to ~100 $\mu$M solution of $^{15}$N-UBA domain (WT, mutant, or hydroxylated) or $^{15}$N-linear diubiquitin and $^{15}$N-monoubiquitin, respectively, to obtain molar ratios between UBA and monoubiquitin moiety of 0, 1:8, 1:4, 1:2, 1, 3:2, 2, 4, 8, and 16. The $^{15}$N,$^{1}$H BEST-TROSY version of heteronuclear single quantum coherence spectroscopy (HSQC) experiments was recorded for the indicated molar ratios at each titration step. Chemical shift perturbation (CSP) analysis was done according to suggestions and formulations from Ref. 43. CSP values were calculated for each individual backbone proton using the formula, $\Delta\delta = (\Delta\delta H^2 + (\Delta\delta N/5)^2)^{1/2}$. The dissociation constants, $K_D$, were calculated by a least-squares fit to the titration data under the assumptions of a fast exchange regime and a one-binding site mode of protein interaction. Structural modeling of the UBA domain was performed using the protein modeling portal (www.proteinmodelportal.org)[3] with the NMR structure of human UBA domain of OTUD7A (PDB code 2L2D, 85% identity) as a template.

### *Mass spectrometry*

To identify hydroxylated Cezanne *in cellulo*, SILAC-labeled HEK293 FIH1 KO cells were transfected with GFP-Cezanne in the absence and presence of exogenous FIH1 under normoxic and hypoxic (1% oxygen, 16 h) conditions (three 10-cm dishes/condition).

Cells were lysed (50 mM Tris-HCl (pH 7.5), 150 mM NaCl, 1% Nonidet P-40, 25 mM NaF, 1× cOmplete, EDTA-free protease inhibitors (Roche Applied Science)). Immunoprecipitation was performed using GFP-Trap®–agarose (Chromotek). Beads were washed five times with lysis buffer, three times with 8 M urea, and subsequently three times with Milli-Q water. An in-solution digest was performed. In brief, protein elution and denaturation were performed by boiling the samples in 6 M guanidine hydrochloride buffer and adding 50 mM ammonium bicarbonate. 10 mM tris(2-carboxyethyl)phosphine and 40 mM chloroacetamide were added to the sample. Proteins were digested with trypsin overnight. Tryptic peptides were desalted and concentrated using STAGE-Tips (Empore C18, 3 M). Peptides were separated on a self-made 15-cm C18 column on an Easy nLC 1200 system (Thermo Fisher Scientific) and injected directly into an Orbitrap Elite mass spectrometer (Thermo Fisher Scientific) that was operated in data-dependent mode. The 20 most abundant peptides were subjected to collision-induced dissociation fragmentation in the linear ion trap after a survey scan in the Orbitrap. Data analysis was done with MaxQuant 1.61 against the Uniprot Human Reference Proteome Database (version 12/17/2017), consisting of 71,775 entries, combined with the MaxQuant Contaminants database (245 entries). Only fully tryptic peptides with a maximum of 2 missed cleavages were taken into account. Modifications were limited to carbamidomethylation of cysteine (fixed) and variable oxidation of methionine, hydroxylation of asparagine, and acetylation of protein N termini. The mass tolerance was set to 20 ppm in the first and 4.5 ppm in the second search for precursor ions and to 0.5 Da for fragment ions. The false discovery rate was set to 1% on peptide-spectrum match (protein and site decoy level). Quantitative information about the abundance of the hydroxylated peptide and its unmodified counterpart were taken from MaxQuant 1.6.1 and analyzed with GraphPad Prism for statistical significance (one-sample *t* test; **, $p \leq 0.01$; ***, $p \leq 0.001$).

To verify hydroxylation of recombinant UBA domain, 3 × 5 $\mu$g of recombinantly expressed and purified His-GST-UBA or His-GST-UBA(Asn$^{35}$OH) was reduced and alkylated in 4% sodium desoxychelate (SDC), 10 mM tris(2-carboxyethyl)phosphine, 40 mM chloroacetamide, pH 8.0, for 10 min at 95 °C. The mixture was cooled down, diluted with 50 mM Tris to 2% SDC, and digested with 0.5 $\mu$g of Lys-C at 37 °C for 1 h. Subsequently, the sample was further diluted to 1% SDC and further digested with 0.5 $\mu$g of trypsin for 5 h at 37 °C. Tryptic peptides were desalted and concentrated using SDB-RPS STAGE-Tips according to Kulak *et al.* (44).

Peptides were separated with a 48-min nonlinear gradient from 0 to 48% acetonitrile on an Easy nLC 1200 system (Thermo Fisher Scientific) with a 20-cm self-packed C18 column and directly injected into a Q Exactive HF (Thermo Fisher Scientific). After a survey scan at 60,000 resolution, the five most abundant precursor ions were fragmented by HCD, and the fragmentation spectra were recorded with a resolution of 30,000. Data analysis was done with MaxQuant 1.6.5 as described above but without SILAC quantification and against a database consisting of the sequence of the tagged UBA construct, supplemented with the MaxQuant contaminants database (245 entries) and the Human Swiss-Prot database (version 9/11/2017). In addition, fragment mass tolerance was set to 0.5 Da. The hydroxylation site was validated by interpretation of manual spectra. Quantitative information about the abundance of the hydroxylated peptide and its unmodified counterpart was taken from MaxQuant and analyzed with GraphPad Prism for statistical significance (one-sample *t* test; **, $p \leq 0.01$; ***, $p \leq 0.001$).

*Author contributions*—J. M., J. H., F. B., V. V. R., and A. B. data curation; J. M., J. H., F. B., V. D., V. V. R., and A. B. formal analysis; J. M. and A. B. validation; J. M. and A. B. investigation; J. M., V. V. R., and A. B. visualization; J. M., J. H., F. B., V. D., and V. V. R. methodology; A. B. conceptualization; A. B. supervision; A. B. funding acquisition; A. B. writing-original draft; A. B. project administration.

*Acknowledgments—We thank Manuel Kaulich for expertise in CRISPR/Cas technology, David Komander and Sonia Rocha for insightful discussions and reagents, Masato Akutsu for reagents and technical advice, Eric Metzen for cell lines, and David Komander and Kerstin Koch for critical reading of the manuscript.*

## References

1. Clague, M. J., Urbé, S., and Komander, D. (2019) Breaking the chains: deubiquitylating enzyme specificity begets function. *Nat. Rev. Mol. Cell Biol.* **20,** 338–352 CrossRef Medline
2. Sahtoe, D. D., and Sixma, T. K. (2015) Layers of DUB regulation. *Trends Biochem. Sci.* **40,** 456–467 CrossRef Medline
3. Bremm, A., Freund, S. M. V., and Komander, D. (2010) $Lys^{11}$-linked ubiquitin chains adopt compact conformations and are preferentially hydrolyzed by the deubiquitinase Cezanne. *Nat. Struct. Mol. Biol.* **17,** 939–947 CrossRef Medline
4. Mevissen, T. E. T., Kulathu, Y., Mulder, M. P. C., Geurink, P. P., Maslen, S. L., Gersch, M., Elliott, P. R., Burke, J. E., van Tol, B. D. M., Akutsu, M., Oualid, F. E., Kawasaki, M., Freund, S. M. V., Ovaa, H., and Komander, D. (2016) Molecular basis of Lys11-polyubiquitin specificity in the deubiquitinase Cezanne. *Nature* **538,** 402–405 CrossRef Medline
5. Pareja, F., Ferraro, D. A., Rubin, C., Cohen-Dvashi, H., Zhang, F., Aulmann, S., Ben-Chetrit, N., Pines, G., Navon, R., Crosetto, N., Köstler, W., Carvalho, S., Lavi, S., Schmitt, F., Dikic, I., *et al.* (2012) Deubiquitination of EGFR by Cezanne-1 contributes to cancer progression. *Oncogene* **31,** 4599–4608 CrossRef Medline
6. Ji, Y., Cao, L., Zeng, L., Zhang, Z., Xiao, Q., Guan, P., Chen, S., Chen, Y., Wang, M., and Guo, D. (2018) The N-terminal ubiquitin-associated domain of Cezanne is crucial for its function to suppress NF-$\kappa$B pathway. *J. Cell. Biochem.* **119,** 1979–1991 CrossRef Medline
7. Enesa, K., Zakkar, M., Chaudhury, H., Luong, L. A., Rawlinson, L., Mason, J. C., Haskard, D. O., Dean, J. L. E., and Evans, P. C. (2008) NF-$\kappa$B suppression by the deubiquitinating enzyme Cezanne: a novel negative feedback loop in pro-inflammatory signaling. *J. Biol. Chem.* **283,** 7036–7045 CrossRef Medline
8. Hu, H., Brittain, G. C., Chang, J.-H., Puebla-Osorio, N., Jin, J., Zal, A., Xiao, Y., Cheng, X., Chang, M., Fu, Y.-X., Zal, T., Zhu, C., and Sun, S.-C. (2013) OTUD7B controls non-canonical NF-$\kappa$B activation through deubiquitination of TRAF3. *Nature* **494,** 371–374 CrossRef Medline
9. Bremm, A., Moniz, S., Mader, J., Rocha, S., and Komander, D. (2014) Cezanne (OTUD7B) regulates HIF-1$\alpha$ homeostasis in a proteasome-independent manner. *EMBO Rep.* **15,** 1268–1277 CrossRef Medline
10. Wang, B., Jie, Z., Joo, D., Ordureau, A., Liu, P., Gan, W., Guo, J., Zhang, J., North, B. J., Dai, X., Cheng, X., Bian, X., Zhang, L., Harper, J. W., Sun, S.-C., and Wei, W. (2017) TRAF2 and OTUD7B govern a ubiquitin-dependent switch that regulates mTORC2 signalling. *Nature* **545,** 365–369 CrossRef Medline
11. Bonacci, T., Suzuki, A., Grant, G. D., Stanley, N., Cook, J. G., Brown, N. G., and Emanuele, M. J. (2018) Cezanne/OTUD7B is a cell cycle-regulated deubiquitinase that antagonizes the degradation of APC/C substrates. *EMBO J.* **37,** e98701 CrossRef Medline
12. Husnjak, K., and Dikic, I. (2012) Ubiquitin-binding proteins: decoders of ubiquitin-mediated cellular functions. *Annu. Rev. Biochem.* **81,** 291–322 CrossRef Medline
13. Mueller, T. D., and Feigon, J. (2002) Solution structures of UBA domains reveal a conserved hydrophobic surface for protein-protein interactions. *J. Mol. Biol.* **319,** 1243–1255 CrossRef Medline
14. Zhou, Z.-R., Gao, H.-C., Zhou, C.-J., Chang, Y.-G., Hong, J., Song, A.-X., Lin, D.-H., and Hu, H.-Y. (2008) Differential ubiquitin binding of the UBA domains from human c-Cbl and Cbl-b: NMR structural and biochemical insights. *Protein Sci.* **17,** 1805–1814 CrossRef Medline
15. Peschard, P., Kozlov, G., Lin, T., Mirza, I. A., Berghuis, A. M., Lipkowitz, S., Park, M., and Gehring, K. (2007) Structural basis for ubiquitin-mediated dimerization and activation of the ubiquitin protein ligase Cbl-b. *Mol. Cell.* **27,** 474–485 CrossRef Medline
16. Matta-Camacho, E., Kozlov, G., Trempe, J. F., and Gehring, K. (2009) Atypical binding of the Swa2p UBA domain to ubiquitin. *J. Mol. Biol.* **386,** 569–577 CrossRef Medline
17. Matsumoto, G., Wada, K., Okuno, M., Kurosawa, M., and Nukina, N. (2011) Serine 403 phosphorylation of p62/SQSTM1 regulates selective autophagic clearance of ubiquitinated proteins. *Mol. Cell.* **44,** 279–289 CrossRef Medline
18. Sowa, M. E., Bennett, E. J., Gygi, S. P., and Harper, J. W. (2009) Defining the human deubiquitinating enzyme interaction landscape. *Cell* **138,** 389–403 CrossRef Medline
19. Ozer, A., and Bruick, R. K. (2007) Non-heme dioxygenases: cellular sensors and regulators jelly rolled into one? *Nat. Chem. Biol.* **3,** 144–153 CrossRef Medline
20. Dames, S. A., Martinez-Yamout, M., De Guzman, R. N., Dyson, H. J., and Wright, P. E. (2002) Structural basis for Hif-1$\alpha$/CBP recognition in the cellular hypoxic response. *Proc. Natl. Acad. Sci. U.S.A.* **99,** 5271–5276 CrossRef Medline
21. Freedman, S. J., Sun, Z.-Y. J., Poy, F., Kung, A. L., Livingston, D. M., Wagner, G., and Eck, M. J. (2002) Structural basis for recruitment of CBP/p300 by hypoxia-inducible factor-1$\alpha$. *Proc. Natl. Acad. Sci. U.S.A.* **99,** 5367–5372 CrossRef Medline
22. Cockman, M. E., Webb, J. D., and Ratcliffe, P. J. (2009) FIH-dependent asparaginyl hydroxylation of ankyrin repeat domain-containing proteins. *Ann. N.Y. Acad. Sci.* **1177,** 9–18 CrossRef Medline
23. Janke, K., Brockmeier, U., Kuhlmann, K., Eisenacher, M., Nolde, J., Meyer, H. E., Mairbäurl, H., and Metzen, E. (2013) Factor inhibiting HIF-1 (FIH-1) modulates protein interactions of apoptosis-stimulating p53 binding protein 2 (ASPP2). *J. Cell Sci.* **126,** 2629–2640 CrossRef Medline
24. Karttunen, S., Duffield, M., Scrimgeour, N. R., Squires, L., Lim, W. L., Dallas, M. L., Scragg, J. L., Chicher, J., Dave, K. A., Whitelaw, M. L., Peers, C., Gorman, J. J., Gleadle, J. M., Rychkov, G. Y., and Peet, D. J. (2015) Oxygen-dependent hydroxylation by FIH regulates the TRPV3 ion channel. *J. Cell Sci.* **128,** 225–231 CrossRef Medline
25. Scholz, C. C., Rodriguez, J., Pickel, C., Burr, S., Fabrizio, J. A., Nolan, K. A., Spielmann, P., Cavadas, M. A. S., Crifo, B., Halligan, D. N., Nathan, J. A., Peet, D. J., Wenger, R. H., Von Kriegsheim, A., Cummins, E. P., and Taylor, C. T. (2016) FIH regulates cellular metabolism through hydroxylation of the deubiquitinase OTUB1. *PLoS Biol.* **14,** e1002347 CrossRef Medline
26. Price, C., Merchant, M., Jones, S., Best, A., Von Dwingelo, J., Lawrenz, M. B., Alam, N., Schueler-Furman, O., and Kwaik, Y. A. (2017) Host FIH-mediated asparaginyl hydroxylation of translocated *Legionella pneumophila* effectors. *Front. Cell. Infect. Microbiol.* **7,** 54 CrossRef Medline
27. Marchler-Bauer, A., Bo, Y., Han, L., He, J., Lanczycki, C. J., Lu, S., Chitsaz, F., Derbyshire, M. K., Geer, R. C., Gonzales, N. R., Gwadz, M., Hurwitz, D. I., Lu, F., Marchler, G. H., Song, J. S., *et al.* (2017) CDD/SPARCLE: functional classification of proteins via subfamily domain architectures. *Nucleic Acids Res.* **45,** D200–D203 CrossRef Medline
28. Loenarz, C., and Schofield, C. J. (2011) Physiological and biochemical aspects of hydroxylations and demethylations catalyzed by human 2-oxoglutarate oxygenases. *Trends Biochem. Sci.* **36,** 7–18 CrossRef Medline
29. Moniz, S., Bandarra, D., Biddlestone, J., Campbell, K. J., Komander, D., Bremm, A., and Rocha, S. (2015) Cezanne regulates E2F1-dependent HIF2$\alpha$ expression. *J. Cell Sci.* **128,** 3082–3093 CrossRef Medline
30. Lancaster, D. E., McNeill, L. A., McDonough, M. A., Aplin, R. T., Hewitson, K. S., Pugh, C. W., Ratcliffe, P. J., and Schofield, C. J. (2004) Disruption of dimerization and substrate phosphorylation inhibit factor inhibiting hypoxia-inducible factor (FIH) activity. *Biochem. J.* **383,** 429–437 CrossRef Medline
31. Walinda, E., Morimoto, D., Sugase, K., Konuma, T., Tochio, H., and Shirakawa, M. (2014) Solution structure of the ubiquitin-associated (UBA)

domain of human autophagy receptor NBR1 and its interaction with ubiquitin and polyubiquitin. *J. Biol. Chem.* **289,** 13890–13902 CrossRef Medline
32. Kelley, L. A., Mezulis, S., Yates, C. M., Wass, M. N., and Sternberg, M. J. E. (2015) The Phyre2 web portal for protein modeling, prediction and analysis. *Nat. Protoc.* **10,** 845–858 CrossRef Medline
33. Sims, J. J., Haririnia, A., Dickinson, B. C., Fushman, D., and Cohen, R. E. (2009) Avid interactions underlie the Lys63-linked polyubiquitin binding specificities observed for UBA domains. *Nat. Struct. Mol. Biol.* **16,** 883–889 CrossRef Medline
34. Vincendeau, M., Hadian, K., Messias, A. C., Brenke, J. K., Halander, J., Griesbach, R., Greczmiel, U., Bertossi, A., Stehle, R., Nagel, D., Demski, K., Velvarska, H., Niessing, D., Geerlof, A., Sattler, M., and Krappmann, D. (2016) Inhibition of canonical NF-κB signaling by a small molecule targeting NEMO-ubiquitin interaction. *Sci. Rep.* **6,** 18934 CrossRef Medline
35. Komander, D., Reyes-Turcu, F., Licchesi, J. D. F., Odenwaelder, P., Wilkinson, K. D., and Barford, D. (2009) Molecular discrimination of structurally equivalent Lys 63-linked and linear polyubiquitin chains. *EMBO Rep.* **10,** 466–473 CrossRef Medline
36. García-Santisteban, I., Bañuelos, S., and Rodríguez, J. A. (2012) A global survey of CRM1-dependent nuclear export sequences in the human deubiquitinase family. *Biochem. J.* **441,** 209–217 CrossRef Medline
37. Dephoure, N., Zhou, C., Villén, J., Beausoleil, S. A., Bakalarski, C. E., Elledge, S. J., and Gygi, S. P. (2008) A quantitative atlas of mitotic phosphorylation. *Proc. Natl. Acad. Sci. U.S.A.* **105,** 10762–10767 CrossRef Medline
38. Wang, L. (2017) Genetically encoding new bioreactivity. *N. Biotechnol.* **38,** 16–25 CrossRef Medline
39. Richardson, J. S., and Richardson, D. C. (1988) Amino acid preferences for specific locations at the ends of α helices. *Science* **240,** 1648–1652 CrossRef Medline
40. Doench, J. G., Fusi, N., Sullender, M., Hegde, M., Vaimberg, E. W., Donovan, K. F., Smith, I., Tothova, Z., Wilen, C., Orchard, R., Virgin, H. W., Listgarten, J., and Root, D. E. (2016) Optimized sgRNA design to maximize activity and minimize off-target effects of CRISPR-Cas9. *Nat. Biotechnol.* **34,** 184–191 CrossRef Medline
41. Rogov, V. V., Rozenknop, A., Rogova, N. Y., Löhr, F., Tikole, S., Jaravine, V., Güntert, P., Dikic, I., and Dötsch, V. (2012) A universal expression tag for structural and functional studies of proteins. *ChemBioChem* **13,** 959–963 CrossRef Medline
42. Salzmann, M., Wider, G., Pervushin, K., Senn, H., and Wüthrich, K. (1999) TROSY-type triple-resonance experiments for sequential NMR assignments of large proteins. *J. Am. Chem. Soc.* **121,** 844–848 CrossRef
43. Williamson, M. P. (2013) Using chemical shift perturbation to characterise ligand binding. *Prog. Nucl. Magn. Reson. Spectrosc.* **73,** 1–16 CrossRef Medline
44. Kulak, N. A., Pichler, G., Paron, I., Nagaraj, N., and Mann, M. (2014) Minimal, encapsulated proteomic-sample processing applied to copy-number estimation in eukaryotic cells. *Nat. Methods.* **11,** 319–324 CrossRef Medline